# The remission status of AML patients after allo-HCT is associated with a distinct single-cell bone marrow T-cell signature

**Mathioudaki et al.**

I. Supplemental Methods
II. Supplemental Figure Legends
III. Supplemental Table Legends

## I. Supplemental Methods

### Sample collection

All patients received a similar immunosuppressive regimen at the time of BM aspiration (calcineurin inhibitor alone or with mycophenolate). For the validation cohort, 338 BM aspirates from 139 AML patients were collected in an unbiased way and retrospectively grouped by time point prior to and post allo-HCT. Cells were processed by red blood cell lysis followed by staining with different antibody cocktails (see Flow cytometry).

### Sample preparation and cell sorting for scRNA-seq

For the scRNA-seq experiment, frozen Ficoll-processed BM samples were thawed at 37°C in a water bath and subsequently transferred to 10 mL pre-warmed thawing media (IMDM Gibco #21980 with 20% FBS (Sigma-Aldrich #F5724) and 0.1 mg/mL DNAse I (Sigma-Aldrich #DN25). Cells were centrifuged at 250 rcf at room temperature for 10 minutes and the pellet was resuspended in 500 µL sorting buffer (1x PBS supplemented with 1% FBS). The concentration of the cell suspension was adjusted to $10^7$ cells/mL and samples were stored on ice. Prior to staining, samples were incubated with Human TruStain FcX (Biolegend #422301) at 4°C for 10 minutes. The samples were subsequently incubated at 4°C for 30 minutes with the following antibodies CD3-PerCP (Biolegend #344814), CD45-Pacific blue (Biolegend #304029), CD34-APC (BD biosciences #555824). Cells were subsequently washed and resuspended in sorting buffer. The final volume of the samples was adjusted to obtain a concentration of 1 - $10x10^6$ cells /mL. Cells were stained using the following antibodies: cells were stained with Caspase 3-FITC (Sartorius, #4440) prior to the sorting. Cells were collected in FACS tubes coated with 10% FBS and collection buffer with 1x PBS and 0.04% RNAse-free BSA (Invitrogen #AM2616).

### scRNA-seq: library preparation & sequencing

Single cells per group across donors were pooled and then used as an input to 10X Genomics single-cell 3′ Gene Expression v3 assay. Libraries were prepared based on manufacturer's instructions. Sequencing was performed using Illumina NextSeq 500.

### scRNA-seq: preprocessing and quality control

Reads were aligned to the GRCh38 reference genome and quantified using cellranger count (10x Genomics, v.3.0.1). The expression data across cells were corrected for ambient RNA using soupX[1]. For the downstream analysis we used Seurat v3 [2]. Cells with less than 200 genes detected and more than 15% mitochondrial genes per cell were filtered out.

### scRNA-seq: normalization and downstream analysis

After quality control and prior to dimensionality reduction, the data were normalized using SCTransform[3], while regressing out the percentage of mitochondrial reads per cell. We first

performed dimensionality reduction using principal component analysis (PCA) on the 3000 most variable features. Ribosomal, mitochondrial, sex chromosome genes and transcripts were excluded from the variable features. Uniform manifold approximation and projection (UMAP) was carried out on the first 50 principal components. Cells were then grouped into clusters using the Louvain algorithm. For defining the resolution (1.5) in FindClusters we used Clustree[4]. Marker genes across the different cell types were identified using Seurat's FindMarkers function on the RNA data slot. Genes considered were detected in at least 50% of cells per cluster (min.pct=0.5). Expression data were imputed using the MAGIC algorithm[5]. Seurat's LabelTransfer analysis was used in order to integrate our in-house scRNA-seq dataset with publicly available PBMCs CITE-seq data[2].

**Donor demultiplexing and sex identification**

Demultiplexing of single cells based on genotypes in order to distinguish donors was performed using souporcell with k = 6[6]. In the scRNA-seq data, the sex of the individuals was defined based on XIST (female) and RPS4Y1 (male) expression (Supplemental Figure 3).

**Enrichment analysis of cell types across conditions**

Per sorted population ($CD3^+$ gate), the enrichment of each cluster was estimated as the odds ratio (OR). P-values were calculated using Fisher's exact test and adjusted for multiple comparisons using the Bonferroni correction method. Per condition, a cluster was considered enriched when log2(OR) was greater than 0 and with a p.adj < 0.05. To ensure that this OR was not driven by an individual patient, we additionally performed an enrichment analysis for each donor separately, testing the enrichment for each donor against all donors from the other group. For clusters where the donor-specific and the overall analysis agreed in terms of directionality, the p-value for a Fisher's exact test, adjusted for multiple testing with Bonferroni correction, was reported from the overall analysis. For clusters where the donor-specific analysis did not agree with the overall analysis, n.s. was reported independently of the p-value from the overall analysis.

**Transcription factor activity analysis**

The pySCENIC workflow[7] was run using an in-house constructed Snakemake pipeline. For gene regulatory network (GRN) inference, we used the GRNBoost2 algorithm from the Arboreto package[8]. SCENIC analysis was performed on the raw scRNA-Seq data. For predicting the transcription factor (TF) regulons, we used human v9 motif collection, hg38__refseq-r80__10kb_up_and_down_tss.mc9nr.feather and hg38__refseq-r80__500bp_up_and_100bp_down_tss.mc9nr.feather databases from cisTarget (https://resources.aertslab.org/cistarget/). The output AUC scores per cell and GRN were used for visualization and downstream analysis. Assignment of target genes to known functions was performed using publicly available gene sets (IFN: HALLMARK_INTERFERON_GAMMA_RESPONSE, HALLMARK_INTERFERON_ALPHA_RESPONSE; Activation: Gene ontology, cell activation involved in immune response and regulation of immune effector process, TNF: HALLMARK_TNFA_SIGNALING_VIA_NFKB).

**Differential expression and transcription factor activity analysis**

For differential expression analysis between conditions we used FindMarkers function on the RNA slot with the method MAST, an algorithm suitable for scRNA-seq differential expression analysis[9]; we identified differentially expressed genes in the 2 T cell populations: $CD4^+$ and $CD8^+$ (p.adj < 0.05 & log2FC > 0.5). In order to identify differentially active transcription factors

(TFs) we used the SCENIC output to reconstruct a GRN and infer TF activity. To detect the enrichment of TFs for therapy response genes we used Fisher's exact test (fdr < 0.05).
Functional analysis of differentially expressed genes was performed using ClusterProfiler[10] (Gene ontology enrichment analysis using enrichGO function; KEGG pathway analysis using compareCluster function), msigdbr[11,12] (Hallmark collection using enricher function) and ReactomePA[13] (pathway annotation using enrichPathway function). The background gene-set was defined as all the genes expressed in the dataset. P values were adjusted using Benjamini-Hochberg and the cutoff was set to 0.05.

**Trajectory analysis**

We calculated the pseudotime of the $CD8^+$ T cells ($CD8^+$ NV, $CD8^+$ eff. 1 and 2, $CD8^+$ mem. 1, 2 and 3) using Monocle3[14], on the SCT assay. Prior to pseudotime analysis, single cells across patients were aligned using align_cds. The function learn_graph was run with the use_partition argument set to True. $CD8^+$ NV cells were set as the starting point. Diffusion maps[15] were computed on the SCT assay using PAGA[16].

**Flow Cytometry analysis**

Bone marrow or peripheral blood samples were lysed in red blood cell lysis solution (0.15 M ammonium chloride, 10 mM potassium bicarbonate and 0.1 mM EDTA, diluted in sterile neutral pH water with a final pH between 7.2 and 7.8) at room temperature for 10 minutes. Subsequently, samples were centrifuged at 250 rcf for 5 minutes and the pellet was washed with 1x PBS (Gibco #14200). Staining was performed in 50-100 µL cell suspension for 15 minutes at room temperature in the dark. After staining, the pellet was washed with 1x PBS and resuspended in 100-200 µL PBS.
Cells were stained using the following antibodies: CD45-Pacific blue (Biolegend #304029), GPR56-PE (Biolegend #358204), CD34-APC (BD biosciences #555824), CD45RA-PECy7 (Biolegend # 304126), CD3-FITC (BD biosciences #555916), CD8-APC (BD biosciences #555369), CD33-PECy5 (BD biosciences #551377), CD4-APCH7 (BD biosciences #560158), CD56-PECy7 (Biolegend #362509), CD27-BV510 (Biolegend #302835), CCR7-Pacific blue (Biolegend #353210), CD62L-BV510 (Biolegend #304843) and CD3-PerCP (Biolegend #344814), CD107a-PE- Cy7 (Biolegend #328618), PD-1-APC (Biolegend #329908), CD69-PerCP (Biolegend #310928), CD44-FITC (Biolegend #163606). PBMCs activation was performed using phorbol myristate acetate (PMA; SigmaAldrich, #P8139-1MG) and ionomycin for 4h (SigmaAldrich, #I0634-1MG) according to the manufacturer's instructions.

**Intracellular flow cytometry analysis**

For the intracellular analysis of GZMB and PRF1, PBMCs of 10 AML patients post allo-HCT were used. Unless stated otherwise, after each step samples were washed with FACS buffer (1x PBS supplemented with 2% FBS; 1200rpm/5min/RT). After thawing, cells were incubated for 15 minutes at room temperature with Zombie yellow (Zombie Yellow: Biolegend, #423103) according to the manufacturer's protocol, followed by a 15 minute staining at room temperature with cell surface antibodies (GPR56-PE, Biolegend #358204; CD3-BUV750, BD Biosciences #747058; CD8-BUV395, BD Biosciences #563795). Cells were then permeabilized using BD Permeabilizing solution 2 (BD Biosciences #340973) for 10 minutes at room temperature and then washed with FACS buffer (1000 g/5 minutes/room temperature). Finally, samples were stained for GZMB (GZMB-PE-Cy5, Biolegend, #372226) and PRF1 (PRF1-PacBlue, Biolegend, #353305) for 15 minutes at room temperature. Flow cytometry analysis was done on a FACSymphony cytometer.

**FACS data analysis**

Cell debris was gated out. Cell singlets were selected using FSC-A over FSC-H and were divided into lymphocytes ($CD45^{high}SSC^{low}$), monocytes ($CD45^{high}SSC^{int}$), granulocytes ($CD45^{high/int}SSC^{high}$) and blasts ($CD45^{low/int}SSC^{low/int}$). Within the lymphocytes, cells were divided into T cells ($CD3^{+}$) and non-T cells (CD3 negative). T cells were subsequently divided into various populations based on the expression of CD4, CD8, CD27, GPR56. Non-T cells were subdivided into $CD56^{-}$ and $CD56^{+}$ populations. Within $CD4^{+}CD8^{-}$ and $CD4^{-}CD8^{+}$ populations, following populations were defined based on the expression level of CCR7 and CD45RA: naive T cells ($CCR7^{+}CD45RA^{+}$), central memory cells (CM, $CCR7^{+}CD45RA^{-}$), effector memory cells (EM, $CCR7^{-}CD45RA^{-}$) and effector memory with CD45RA expression (EMRA, $CCR7^{-}CD45RA^{+}$). When patients were sampled several times, we consistently used the latest available time point per patient per analyzed time interval.

**CAR-T cell experiments**

For the production of the CD33-specific 3G (28.4-1BB.CD3z) CAR retroviruses[17], 293T cells were co-transfected with the specific retroviral packaging plasmid, PegPam 3 plasmid (containing gag-pol) and RDF plasmid (containing the envelope) followed by harvest of the generated retroviral supernatants. Cells were cultured with IL-7/IL-15 (R&D Systems, Minneapolis, MN, USA). CD33.CAR-T cells were harvested on day 14 of expansion and challenged with HL60 cells as part of a long-term co-culture assay. Non-transduced ATCs were used as negative controls.

CARTs or non-transduced T cells (NTCs) were co-cultured with leukemic HL60 cells in 96-well plates in the absence of exogenous cytokines. The ratio of effector cells to leukemia cells was fixed at 1:1 on day 0, with $2{,}5x10^{4}$ cells of each kind per well. We harvested one well per condition every 5 days and calculated the total number of T-cells and HL60 cells by flow cytometry using CountBright beads (Invitrogen). The dead cell population was excluded by 7-AAD staining. HL60 cells were identified by ZsGreen expression. If HL60 cells were eliminated, T-cells were re-challenged with the same number of fresh HL60 cells that were initially used.

On days 5 and 10 of the co-culture experiment, each technical replicate was transferred to a larger well (48-well plate and 24-well plate, respectively) in order to accommodate the rapidly growing CAR-T population.

For the sorting experiment, CD33.CAR-T cells were harvested from co-cultures after the first challenge, sorted for $CD8^{+}$ and $GPR56^{+/-}$ and $CD27^{+/-}$ on a BD Aria II sorter. After a 24h rest-period the sorted fractions were re-exposed to HL60 cells. Cultures were assessed by flow cytometry at the end of the 5-day co-culture periods. HL60 CD33 KO cells were generated as described[17]. HL-60 (#ACC 3) were purchased from Leibniz Institute DSMZ-German Collection of Microorganisms and Cell Cultures, Braunschweig, Germany.

**ELISpot assay**

$CD8^{+}$ T cells from healthy PBMC donors were sorted into a $GPR56^{+}$ and $GPR56^{-}$ fraction on a BD Aria II cell sorter (Becton Dickinson, Franklin Lakes, NJ). Immediately after sorting, the T cell populations were immersed in pre-warmed RPMI-1640 media supplemented with 10% HI-FBS and 10ng/ml IL-15 (Peprotech, Cat.: Nr. 200-15) to support their viability after sorting. The cells incubated overnight and thoroughly washed to remove traces of IL-15 prior to the start of co-culture in the next morning. The ELISPOT assay was performed in accordance with the manual provided by the manufacturer (MabTech, Cat.: Nr. 3420-4HPW-2). After unsealing, the ELISPOT 96-well plate was thoroughly washed with sterile PBS, then blocked with RPMI

1640 (Sigma-Aldrich #R8758) containing 10% FBS as was used during the co-culture. In the co-culture step, the medium was removed, and a mixture of effector and target cells was added to each well at a ratio of 1:4 (25,000 effector cells and 100,00 AML cells per well). Positive controls consisted of T cells only, stimulated with a monoclonal anti-CD3 antibody (1:1000 dilution, mAb CD3-2). Negative controls consisted of effectors only, resuspended in complete medium without further additives. The plate was then placed in a 37°C incubator with 5% CO2 for 24 hours. For the detection of the secreted IFNγ, cells were removed, and the plate was washed 5 times with 1x PBS. The staining procedure included an incubation with a biotinylated primary anti-IFNγ (mAb 1-D1K) monoclonal antibody, followed by a wash and a secondary Streptavidin-HRP conjugate. Finally, a TMB solution was added and left to react for 3 minutes at room temperature, as dark spots formed on the membrane. The color development was stopped by extensive washing in deionized water. The plate was then left to dry at room temperature in the dark. The spots were counted and the plate analyzed using an ELISPOT reader.

## II. Supplemental Figure Legends

**Supplemental Figure 1: FACS gating strategy for scRNA-seq analysis.**
Gating strategy used to isolate $CD3^+$ T cells and $CD34^+$ HSPCs from bone marrow aspirates prior to 10x scRNA-seq.

**Supplemental Figure 2: Quality control of single cell RNA-seq data.**
(A, B) Number of genes relative to count depth colored by the fraction of mitochondrial reads (% of mito reads) prior quality control (QC; A) and post QC (B).
(C) Number of cells per sample.
(D) Number of genes per cell per sample.
(E) Number of unique molecular identifiers (UMIs) in a log2 scale.
(F) Percentage of mitochondrial reads per cell.

**Supplemental Figure 3: Sex annotation per donor, based on scRNA-seq data.**
Violin plots showing the normalized expression of XIST (X linked gene, female) and RPS4Y1 (Y chromosome gene, male) per patient sample.

**Supplemental Figure 4: Patient representation of identified populations.**
(A) UMAP representing 4 major identified populations.
(B) Barplots indicating the fractions of the different populations per patient sample.
(C) Sample representation per cell type/state within the $CD34^+$ subsets (log10-scale).
(D) Sample representation per cell type/state within the T cell subsets (log10-scale).
(E) (Top) Differential abundance analysis per cell type/state within the $CD3^+$ T-cells using Fisher's exact test (same as Figure 2C for easier comparison). The bars represent the log2 odds ratios of CR vs REL samples. (Bottom) Differential abundance analysis per sample and cell type within the $CD3^+$ T cell compartments using Fisher's exact test. The colors represent the log2 odds ratios of one sample (y-axis) vs all samples from the opposite condition (p-values were adjusted for multiple comparisons using the Bonferroni correction method), n.s.: not significant, *P < 0.05, **P < 0.001, ***P < 0.0001).

**Supplemental Figure 5: Transcriptome levels across conventional $CD8^+$ cell pseudotime.**
(A) $CD8^+$ UMAP created using Monocle3. The different colors indicate the different clusters.

(B) UMAP colored by pseudotime as inferred from Monocle3. Gray points indicate the disconnected cells, computationally excluded from the pseudotime analysis.
(C) Normalized expression of GZMK, NKG7, GNLY and GZMB projected on diffusion maps and split per condition.

**Supplemental Figure 6: Differential expression analysis in CD8$^+$ and CD4$^+$ T cells.**
(A) Volcano plot illustrating the differentially expressed genes between CR and REL samples after selecting all CD8$^+$ subsets. Horizontal dotted lines represent adjusted p value = 0.05 (after Bonferroni correction) and vertical dotted lines represent absolute log2FC > 1.
(B) Volcano plot illustrating the differentially expressed genes between CR and REL after selecting all CD4$^+$ clusters. Horizontal dotted lines represent adjusted p value = 0.05 (after Bonferroni correction) and vertical dotted lines represent absolute log2FC > 1.
(C) Upset plot indicating the overlap of DEGs between the 2 populations (absolute log2FC > 1, p.adj < 0.05 after Bonferroni correction).

**Supplemental Figure 7: SCENIC workflow for extracting differentially active TFs.**
(A) Method overview.
(B) Upset plot indicating the overlap of the differentially active transcription factors (TFs) between the 3 major populations.
(C, D) Bar graphs depicting the log2OR per TF in CD8 (C) and CD4 (D) cells calculated with Fisher's test according to the workflow outlined in A. Green color indicates FDR < 0.05.

**Supplemental Figure 8: Characterization of regulons across TFs in the 3 major cell subsets.**
(A) Upset plot indicating the overlap of target genes across the significantly differentially active TFs.
(B) Venn diagrams representing the overlap of target genes between CD4$^+$ and CD8$^+$ cells for MAFF, JUNB, CREM.

**Supplemental Figure 9: Gene expression changes in MAIT cells and naive CD8$^+$ cells.**
(A, B) Volcano plots illustrating the differentially expressed genes between CR and REL CD8$^+$ NV (A) and MAIT (B) cells. Horizontal dotted lines represent adjusted p value = 0.05 (after Bonferroni correction) and vertical dotted lines represent absolute log2FC > 0.5.

**Supplemental Figure 10: *GPR56* and *CD27* expression along the CD8$^+$ T cells trajectory.**
(A) Density plot indicating the distribution of the normalized expression of *ADGRG1*/*GPR56* and *CD27* within the CD8$^+$ effector memory (EM) cells. Vertical red line indicates the threshold (0.5) used for defining a cell as GPR56$^+$ and CD27$^+$ cells for Figure 3.
(B) Scaled expression across pseudotime of *GPR56*, *CD27* and other CD8$^+$ markers.
(C) Diffusion maps for the CD8$^+$ cells colored by normalized expression of *CD27*, *GPR56* and *ZNF683* and split per condition.
(D) Violin plot depicting the MAGIC imputed expression of *ADGRG1/GPR56* on CD4+ T cells and CD8$^+$ T subsets, split per condition.
(E) Waterfall plot depicting Pearson correlation analysis of *GPR56* expression with other genes in CD8$^+$ TEM cells. The x-axis represents the top 50 correlating genes, while the y-axis shows the Pearson correlation coefficient values. The color-coded scheme distinguishes between positive and negative correlations, with purple bars indicating positive correlations while the orange bars denote negative correlations.

(F) Gene ontology enrichment analysis performed on differentially expressed genes between GPR56$^+$ and GPR56$^-$ CD8$^+$ EM cells.

**Supplemental Figure 11: Gating scheme for intracellular staining.**
Representative scheme illustrating the FACS gating strategy used to separate GPR56$^+$ from GPR56$^-$ CD8$^+$ T cells. The two fractions were further analyzed for PRF1 and GZMB intracellular protein expression. Analysis was performed on PBMCs from a cohort of 10 AML patients in remission.

**Supplemental Figure 12: GPR56 is not redundant with T cell activation markers.**
(A, B) Representative FACS plots illustrating the gating strategy used to separate GPR56$^+$ and GPR56$^-$ fractions for further analysis of CD69 and CD44-(A) and PD-1 and CD107a (B) in the two fractions.
(C, D, E, F) Boxplots illustrating the comparison between the CD8$^+$ GPR56$^+$ (purple) and CD8$^+$ GPR56$^-$ (orange) fractions with regards to percentage of CD44$^+$, CD107a$^+$, PD-1$^+$ and CD69$^+$ fractions, respectively. Connected points indicate fractions originating from the same sample. P-value was calculated using a paired Wilcoxon test. Analysis was performed on PBMCs from a cohort of 10 AML patients in remission.
(G) CD69 and GPR56 profiles of unstimulated (left) PBMC-derived CD8$^+$ T cells as well as after stimulation with PMA and Ionomycin for 4h (right).

**Supplemental Figure 13: GPR56 expression on CAR-T cells.**
(A) Time course of the percentage of CD8$^+$, CD4$^+$, and CD15$^+$ HL60 cells of all viable cells in the cocultures. Cocultures were analyzed every 5 days followed by reexposure to fresh HL60 cells.
(B) Representative FACS histogram plot showing the shift in GPR56 expression on CAR-T cells when exposed to HL60 cells.
(C) Boxplot depicting the percentage of GPR56$^+$ cells within healthy donor CD8$^+$ T cells, without any stimulation (non-activated), after stimulation with anti-CD3 antibody (anti-CD3) and after stimulation with anti-CD3/anti-CD28 antibodies (anti-CD3/anti-CD28). Cells were isolated from PBMCs of 4 healthy donors. Connected points represent samples originating from the same donor. Numbers indicate p-values calculated using paired Wilcoxon test.
(D) Distribution of the percentage of GPR56 and CD27 during the 5 serial challenges. Stacked bars represent the means of the four donors.

**Supplemental Figure 14: Gating strategy for flow cytometry analysis.**
(A) Schematic illustration of the sample work flow.
(B) Gating strategy for panels 1 and 2 as indicated. See supplemental methods for antibody details.
(C) Gating strategy for panel 3. After gating out debris and doublets, gates were set around putative lymphocytes, monocytes and granulocytes according to the typical FSC and SSC pattern. CD3$^+$ T cells were gated from the lymphocyte gate followed by gating for CD4 and CD8. CD8 cells were further analyzed using CCR7 and CD45RA to distinguish naive, central memory ($T_{CM}$), effector memory ($T_{EM}$) and CD45RA$^+$ effector memory ($T_{EMRA}$) T cells. Subsequently, GPR56 positivity was calculated within each of these subsets.

**Supplemental Figure 15: Flow cytometry of patient bone marrow samples.**
(A) Box plot showing median, quartiles, and individual values of GPR56 expression in CD8$^+$ naive and central memory (CM) T cells as well as CD4$^+$ naive, CM, effector memory (EM) and

CD45RA$^+$ EM (EMRA) T cells in patients without (noAllo), before (preAllo), and after (postAllo) allo-HCT. Numbers below plots indicate sample size, values besides box plot indicate the median.
(B) Right panel: percentage of CD8$^+$ $T_{EMRA}$ in bone marrow (left) and percentage of GPR56$^+$ on CD8$^+$ $T_{EMRA}$ (right). Numbers below plots show the median percentage. Numbers between groups of patients without (noAllo), before (preAllo) and after (postAllo) allo-HCT indicate the adjusted p-values (unpaired Wilcoxon test).
(C) Box plot showing median, quartiles, and individual values of GPR56 expression in CD3$^+$CD4$^-$CD8$^-$ double negative T cells (left) and CD3$^-$CD56$^+$ NK cells (right) in patients without (noAllo), before (preAllo), and after (postAllo) allo-HCT. Numbers below plots indicate sample size, values besides box plot indicate the median. Colored numbers above the plot indicate sample numbers.
(D) Time course of GPR56 expression on double negative CD3$^+$CD4$^-$CD8$^-$ T cells (top) and NK cells (bottom). Box plots show medians, quartiles, outliers. Numbers above boxes indicate the medians. Colored numbers above the plot indicate sample numbers.
(E) Time course of GPR56 expression on CD4$^+$ $T_{EMRA}$ (upper) and CD3-CD56$^+$ NK cells (lower) in CMV negative (left) and positive (right) recipients. Box plots show medians, quartiles, outliers. Numbers above boxes indicate the medians.

**Supplemental Figure 16: Time course analysis of patient bone marrow samples.**
(A) Time course for the percentage of GPR56$^+$CD27$^-$ of CD8$^+$ (violet), GPR56$^+$CD27$^+$ of CD8$^+$ (blue), GPR56 of $T_{EM}$ (dark green), and GPR56 of $T_{EMRA}$ (light green) for patient GXW009, GXW097, GXW023, and GXW147. CMV status of patient ("R") and donor ("D"), as well as donor sex are indicated. Text below x-axis indicates clinical course of the disease: CR= complete remission, CRi= complete remission with incomplete recovery, IS= under immunosuppression. Chim= donor chimerism, G-CSF= granulocyte-colony stimulating factor.
(B) Left four panels: Percentage of GPR56 in total CD8$^+$ compartment, CD8$^+$ $T_{EMRA}$, CD4$^+$ and NK cells in patients sampled within the first six months post allo-HCT, who were in CR at sampling and either stayed in CR at last follow-up ("CR") or relapsed at last follow-up ("REL"). Right: Interval between sampling time and allo-HCT in CR and REL group. Colors of dots represent CMV recipient status. Box plots showing median, quartiles, individual values. P-values estimated with Wilcoxon test.

**Supplemental Figure 17: ELISPot assays of post-allo-HCT PBMC derived T cells of CR patients.**
(A) Gating strategy of PBMCs in order to obtain GPR56$^+$ (purple) and GPR56$^-$ (orange) CD8$^+$ fractions of T cells.
(B) Images of ELISpot data summarized in Figure 5I per patient.
(C) Images of ELISpot assay results for GPR56$^+$ and GPR56$^-$ CD8$^+$ T cells of PT6 co-cultured with non-matched primary AML blasts.

## III. Supplemental Table Legends

Supplemental Table 1: Patient and sample characteristics.
Supplemental Table 2: Marker genes of scRNAseq data clusters.
Supplemental Table 3: Cluster abundances using Fisher's exact test.
Supplemental Table 4: Differentially expressed genes between CR and REL in CD8$^+$ and CD4$^+$ T cells.

Supplemental Table 5: SCENIC gene regulatory network.
Supplemental Table 6: Differential TF activity analysis.
Supplemental Table 7: Differentially expressed genes between CR and REL.
Supplemental Table 8: Results from functional enrichment analysis of differentially expressed genes in $CD8^+$ EM cells.
Supplemental Table 9: Differentially expressed genes between $GPR56^+$ and $GPR56^-$ in $CD8^+$ EM in CR.
Supplemental Table 10: Results from functional enrichment analysis of differentially expressed genes between $GPR56^+$ and $GPR56^-$ CR $CD8^+$ EM cells.
Supplemental Table 11: ELISpot results.

## Bibliography


1. Young MD, Behjati S. SoupX removes ambient RNA contamination from droplet-based single-cell RNA sequencing data. *Gigascience*. 2020;9(12):giaa151.

2. Hao Y, Hao S, Andersen-Nissen E, et al. Integrated analysis of multimodal single-cell data. *Cell*. 2021;184(13):3573-3587.

3. Hafemeister C, Satija R. Normalization and variance stabilization of single-cell RNA-seq data using regularized negative binomial regression. *Genome Biol.* 2019;20(1):296.

4. Zappia L, Oshlack A. Clustering trees: a visualization for evaluating clusterings at multiple resolutions. *Gigascience*. 2018;7(7):giy083.

5. van Dijk D, Sharma R, Nainys J, et al. Recovering Gene Interactions from Single-Cell Data Using Data Diffusion. *Cell*. 2018;174(3):716-729.e27.

6. Heaton H, Talman AM, Knights A, et al. Souporcell: robust clustering of single-cell RNA-seq data by genotype without reference genotypes. *Nat. Methods*. 2020;17(6):615–620.

7. Van de Sande B, Flerin C, Davie K, et al. A scalable SCENIC workflow for single-cell gene regulatory network analysis. *Nat. Protoc.* 2020;15(7):2247–2276.

8. Moerman T, Aibar Santos S, Bravo González-Blas C, et al. GRNBoost2 and Arboreto: efficient and scalable inference of gene regulatory networks. *Bioinformatics*. 2019;35(12):2159–2161.

9. Finak G, McDavid A, Yajima M, et al. MAST: a flexible statistical framework for assessing transcriptional changes and characterizing heterogeneity in single-cell RNA sequencing data. *Genome Biol.* 2015;16:278.

10. Wu T, Hu E, Xu S, et al. clusterProfiler 4.0: A universal enrichment tool for interpreting omics data. *Innovation (Camb)*. 2021;2(3):100141.

11. Subramanian A, Tamayo P, Mootha VK, et al. Gene set enrichment analysis: a knowledge-based approach for interpreting genome-wide expression profiles. *Proc Natl Acad Sci USA*. 2005;102(43):15545–15550.

12. Liberzon A, Subramanian A, Pinchback R, et al. Molecular signatures database (MSigDB) 3.0. *Bioinformatics*. 2011;27(12):1739–1740.

13. Yu G, He Q-Y. ReactomePA: an R/Bioconductor package for reactome pathway analysis and visualization. *Mol. Biosyst.* 2016;12(2):477–479.

14. Trapnell C, Cacchiarelli D, Grimsby J, et al. The dynamics and regulators of cell fate decisions are revealed by pseudotemporal ordering of single cells. *Nat. Biotechnol.* 2014;32(4):381–386.

15. Haghverdi L, Buettner F, Theis FJ. Diffusion maps for high-dimensional single-cell analysis of differentiation data. *Bioinformatics*. 2015;31(18):2989–2998.

16. Wolf FA, Hamey FK, Plass M, et al. PAGA: graph abstraction reconciles clustering with trajectory inference through a topology preserving map of single cells. *Genome Biol.* 2019;20(1):59.

17. Liu Y, Wang S, Schubert M-L, et al. CD33-directed immunotherapy with third-generation chimeric antigen receptor T cells and gemtuzumab ozogamicin in intact and CD33-edited acute myeloid leukemia and hematopoietic stem and progenitor cells. *Int. J. Cancer*. 2022;150(7):1141–1155.

**Supplemental Figure 1**

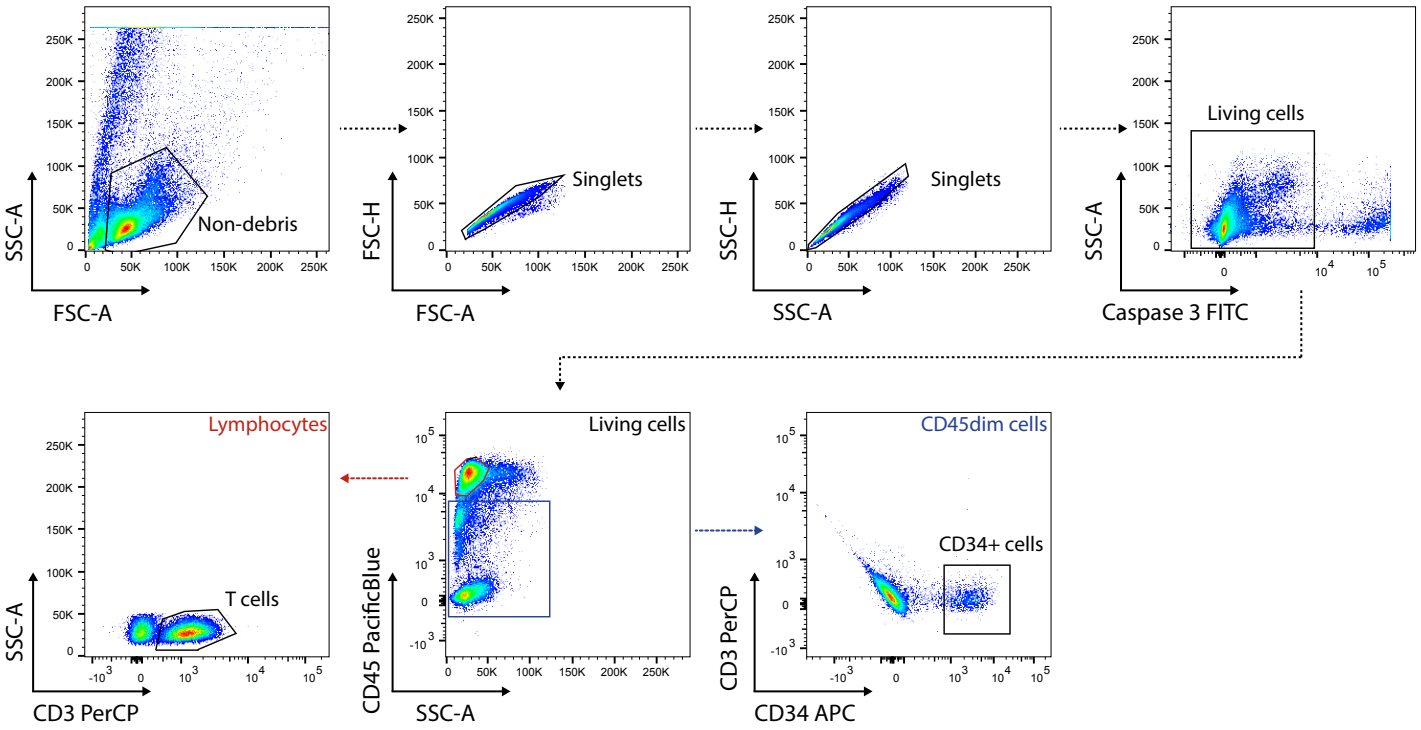

**Supplemental Figure 2**

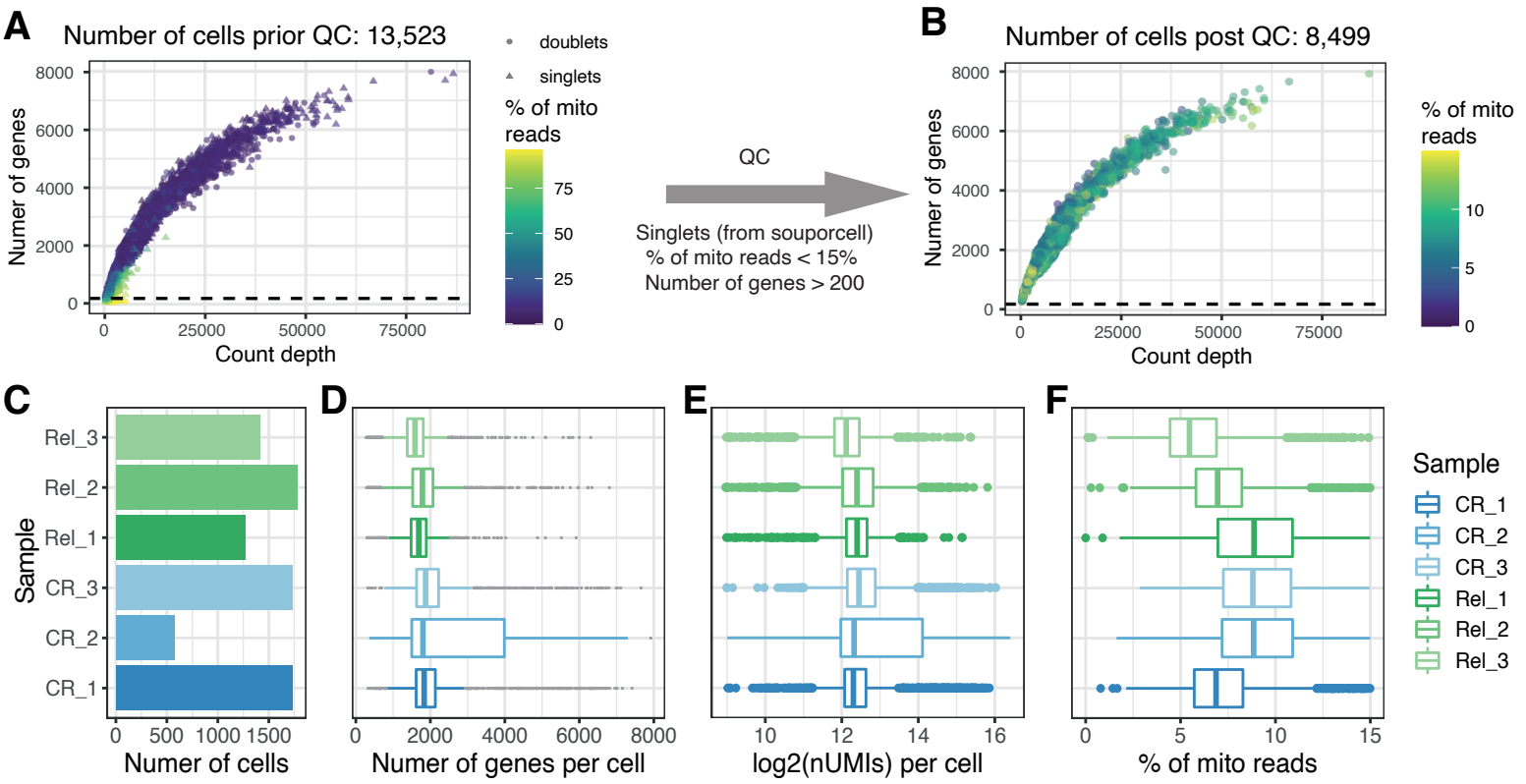

**Supplemental Figure 3**

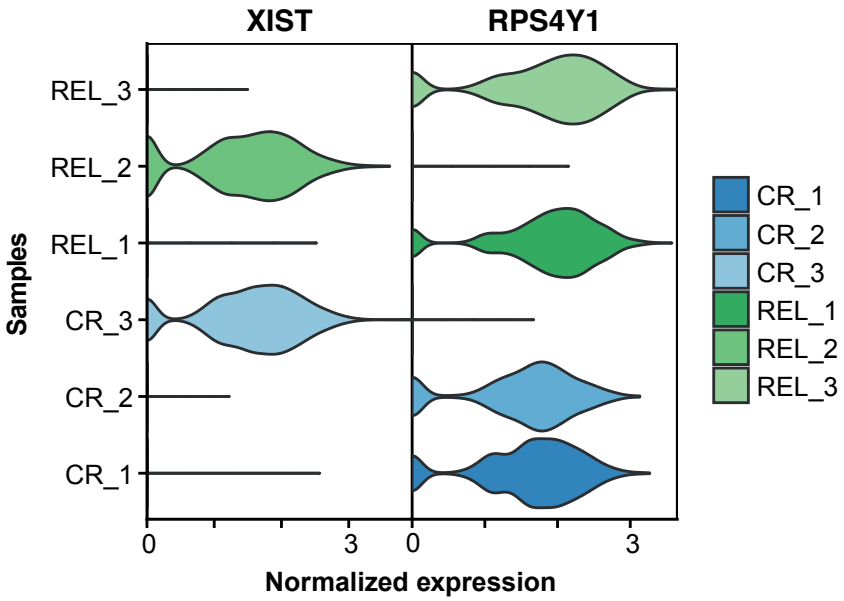

**Supplemental Figure 4**

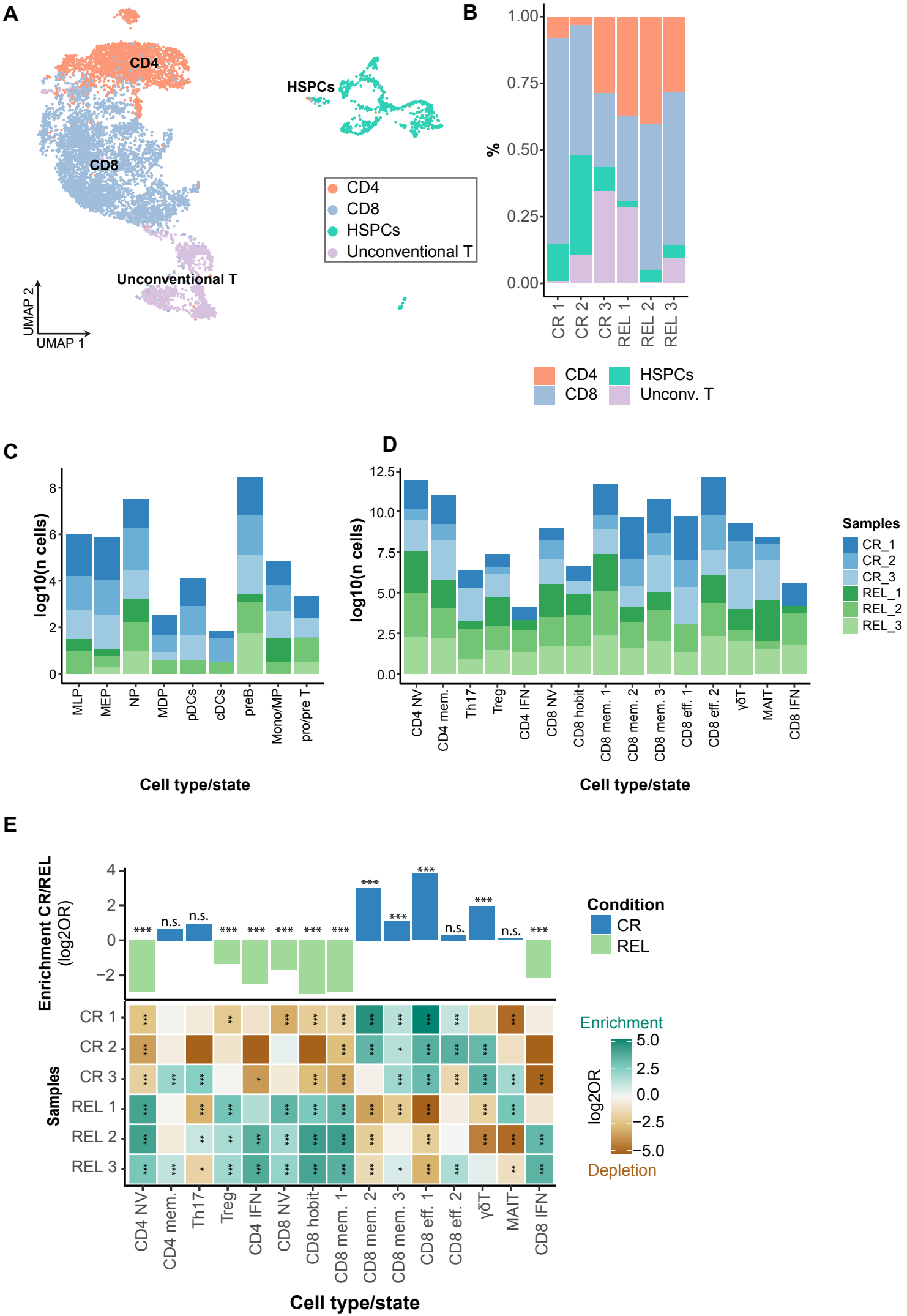

**Supplelemental Figure 5**

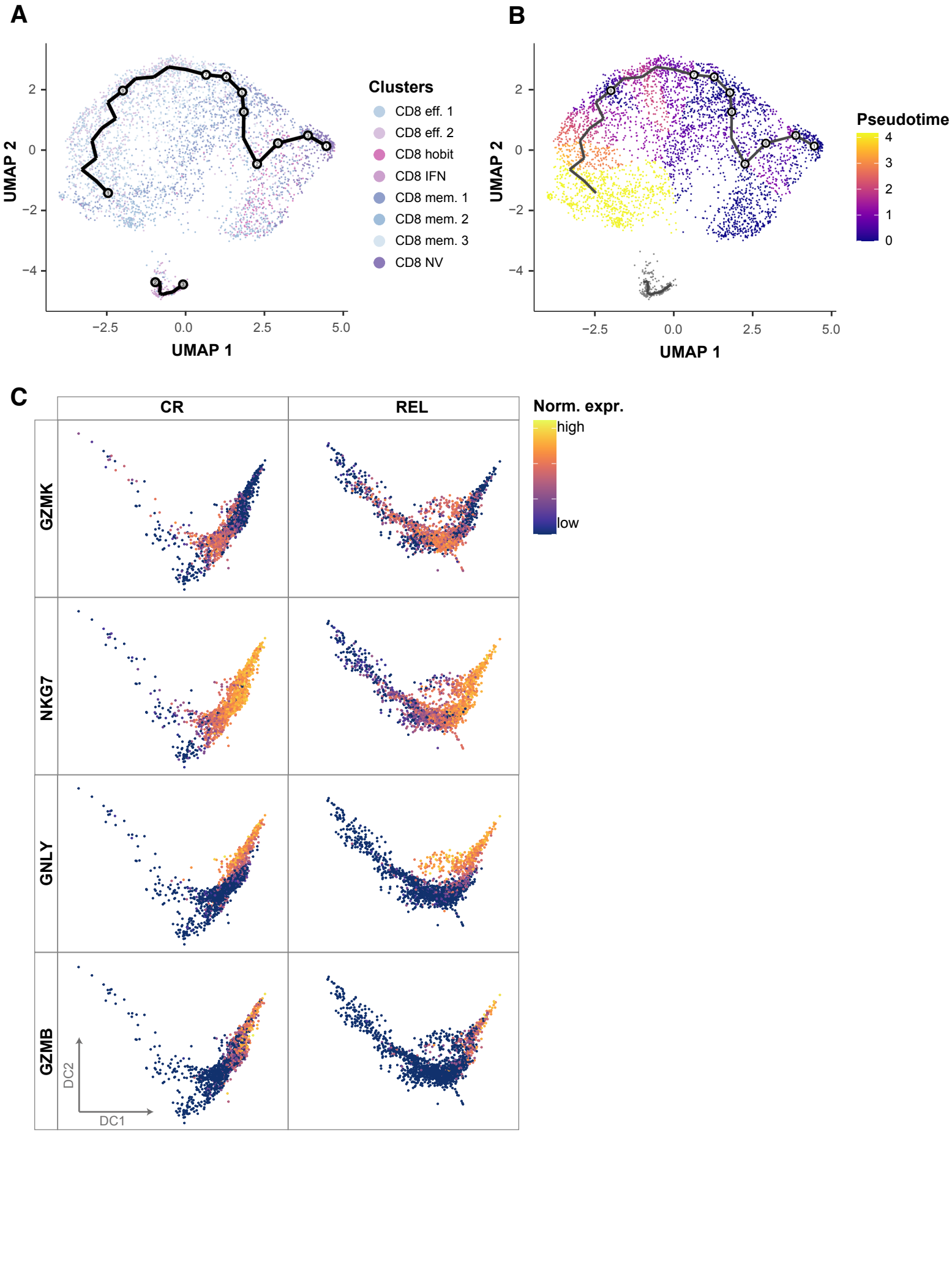

**Supplemental Figure 6**

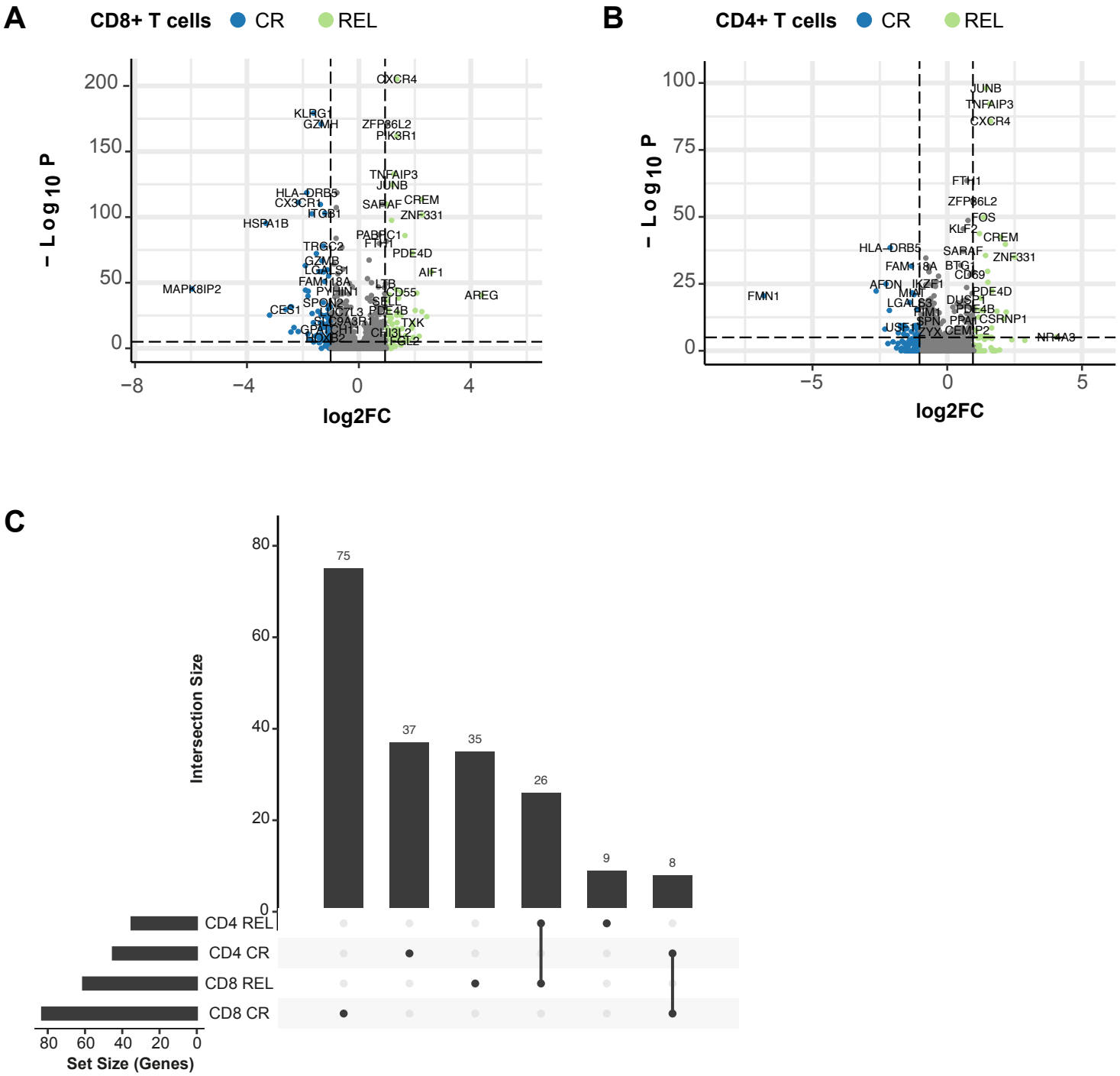

**Supplemental Figure 7**

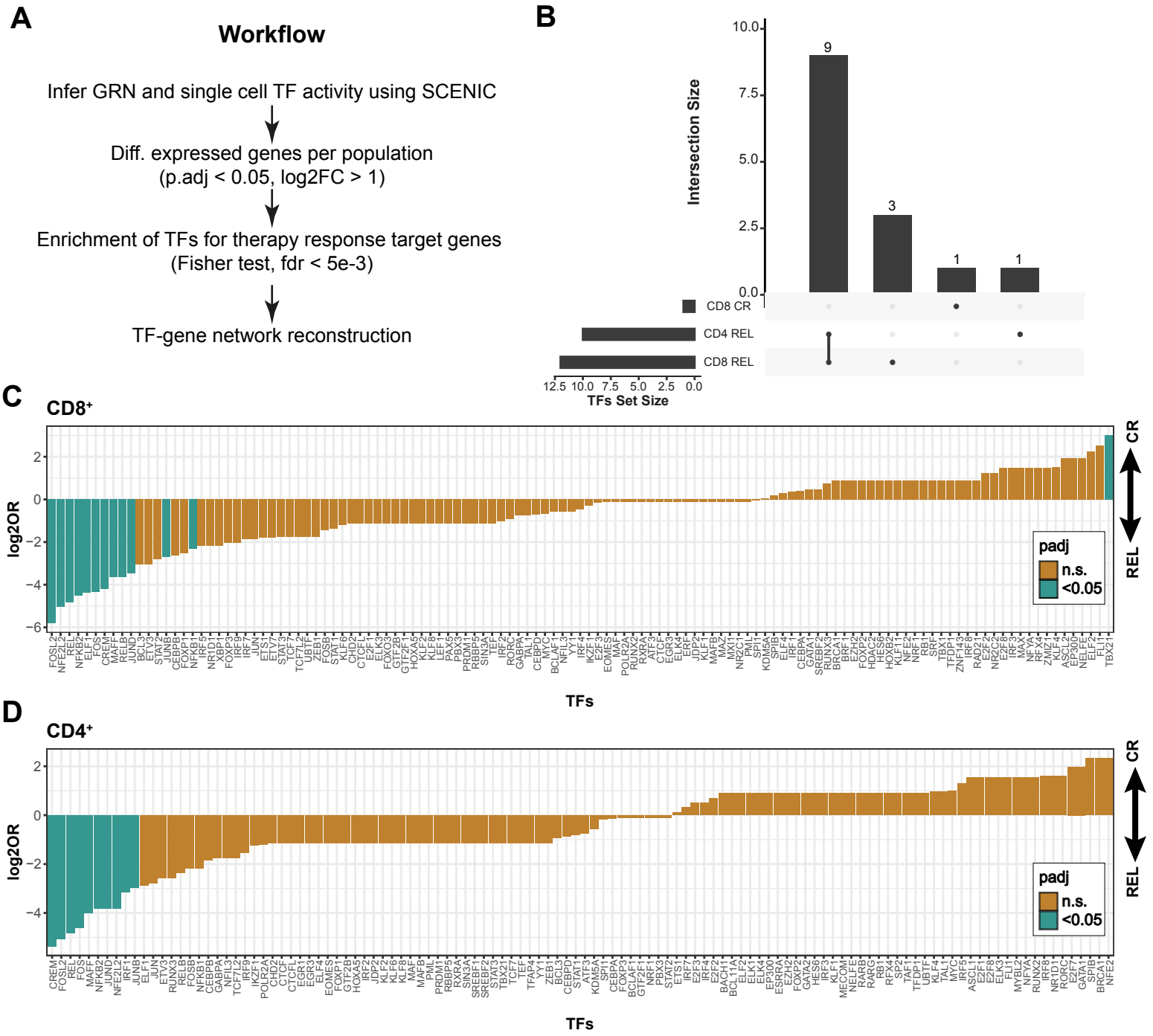

**Supplemental Figure 8**

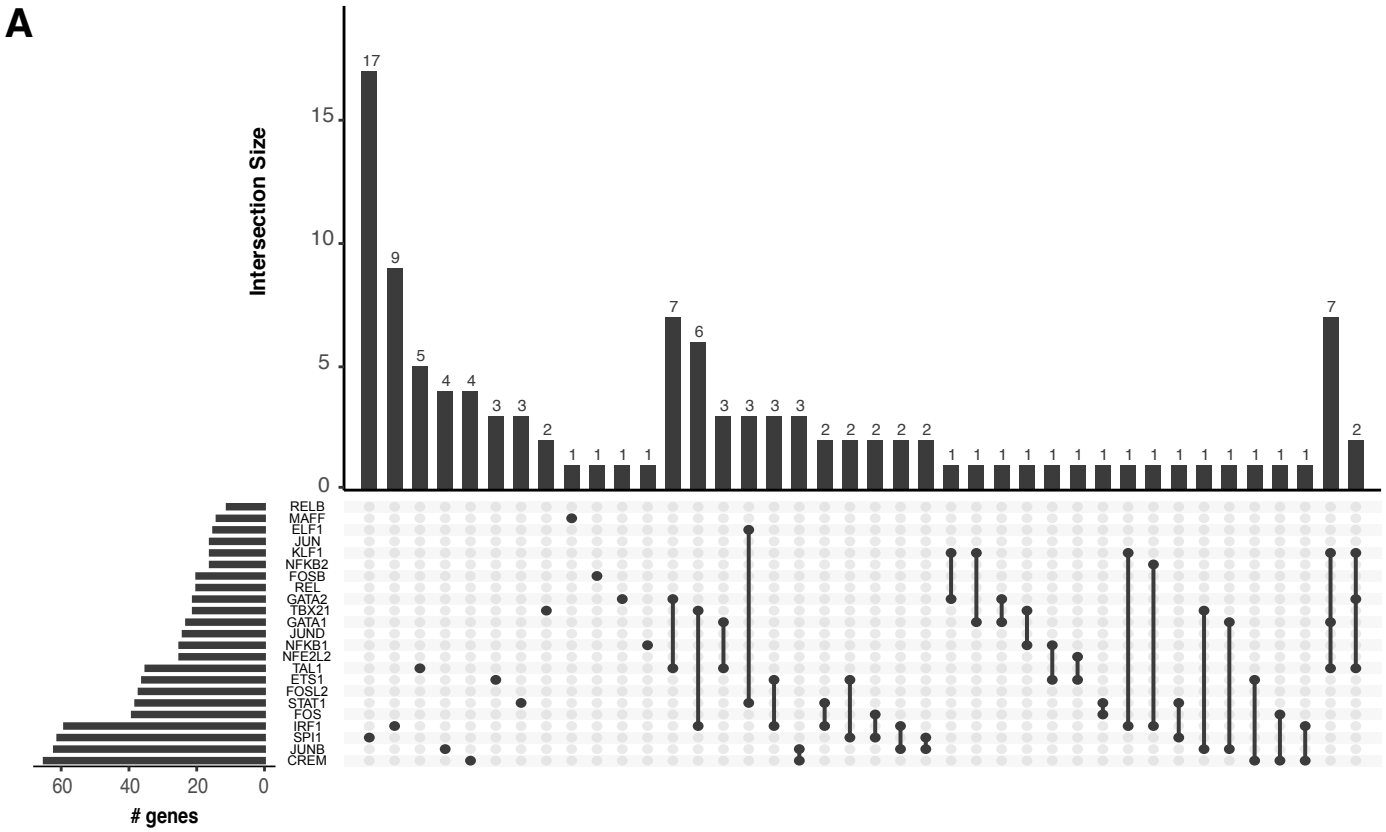


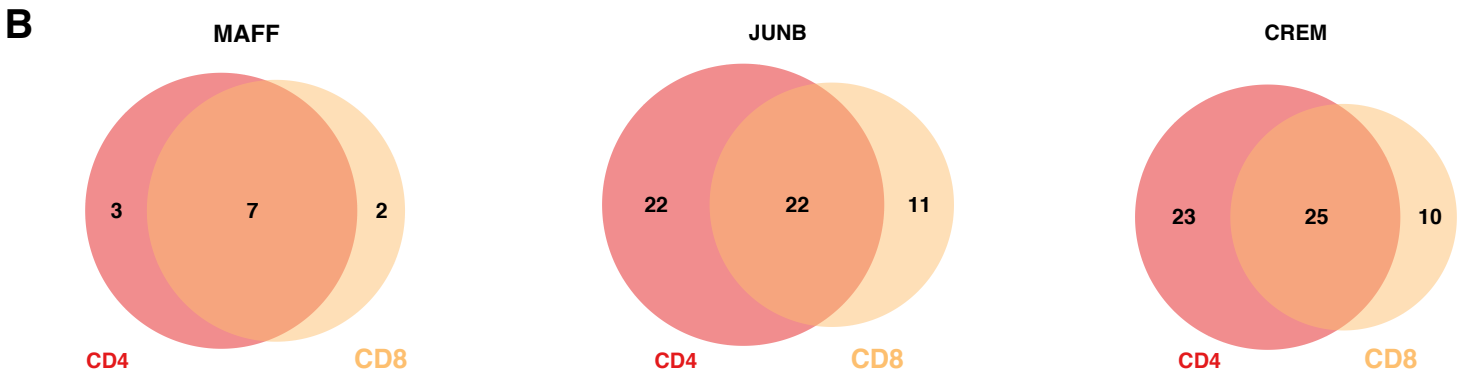

**Supplemental Figure 9**

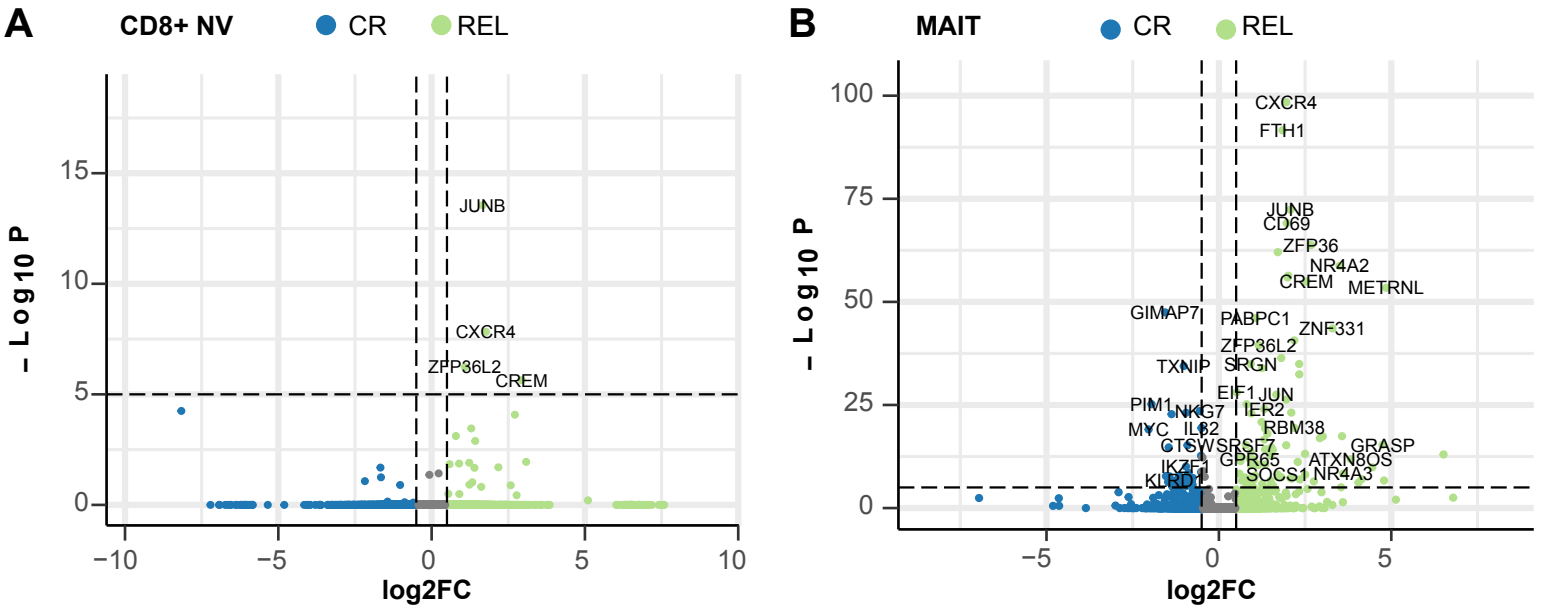

## Supplelemental Figure 10

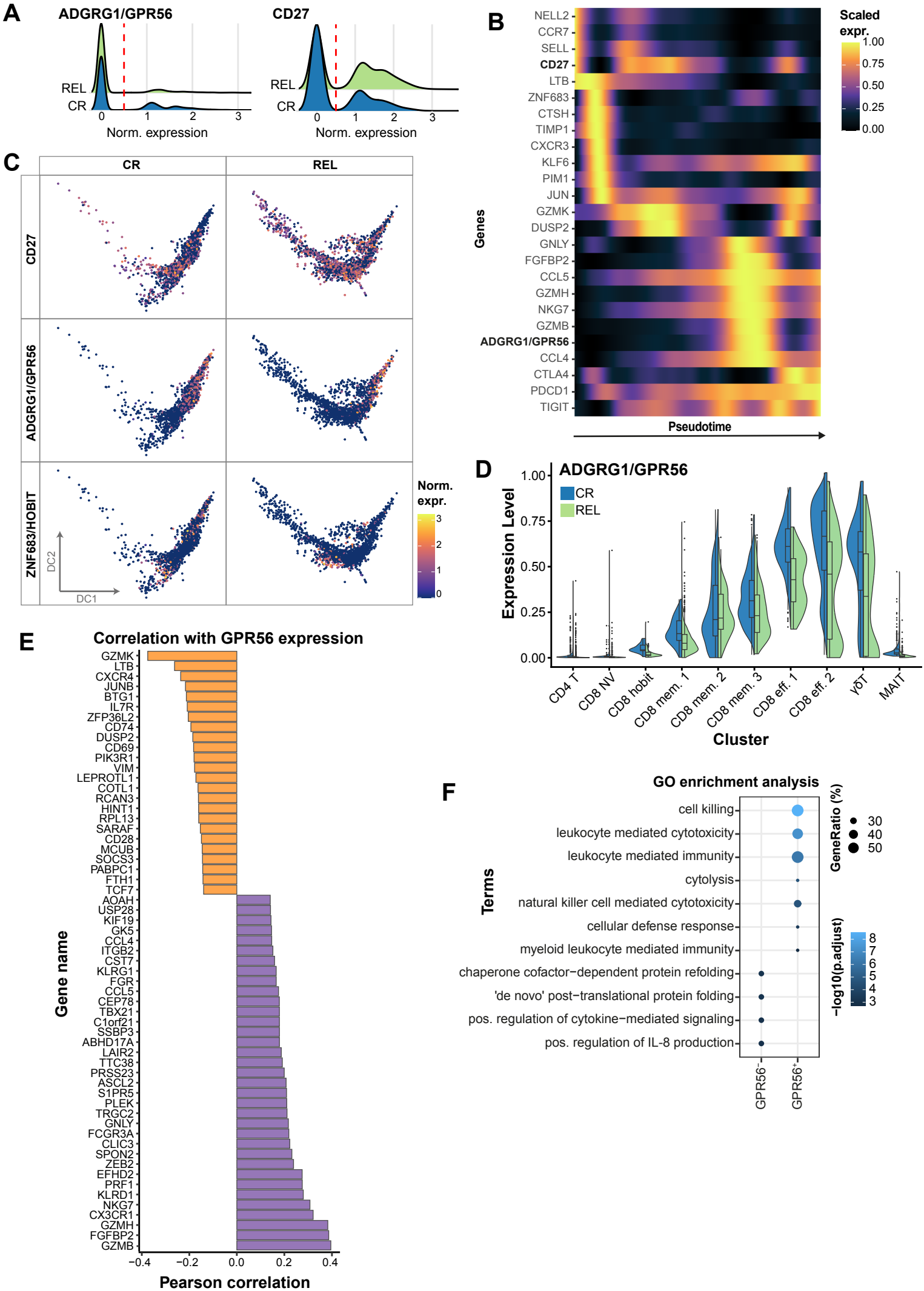

# Supplemental Figure 11

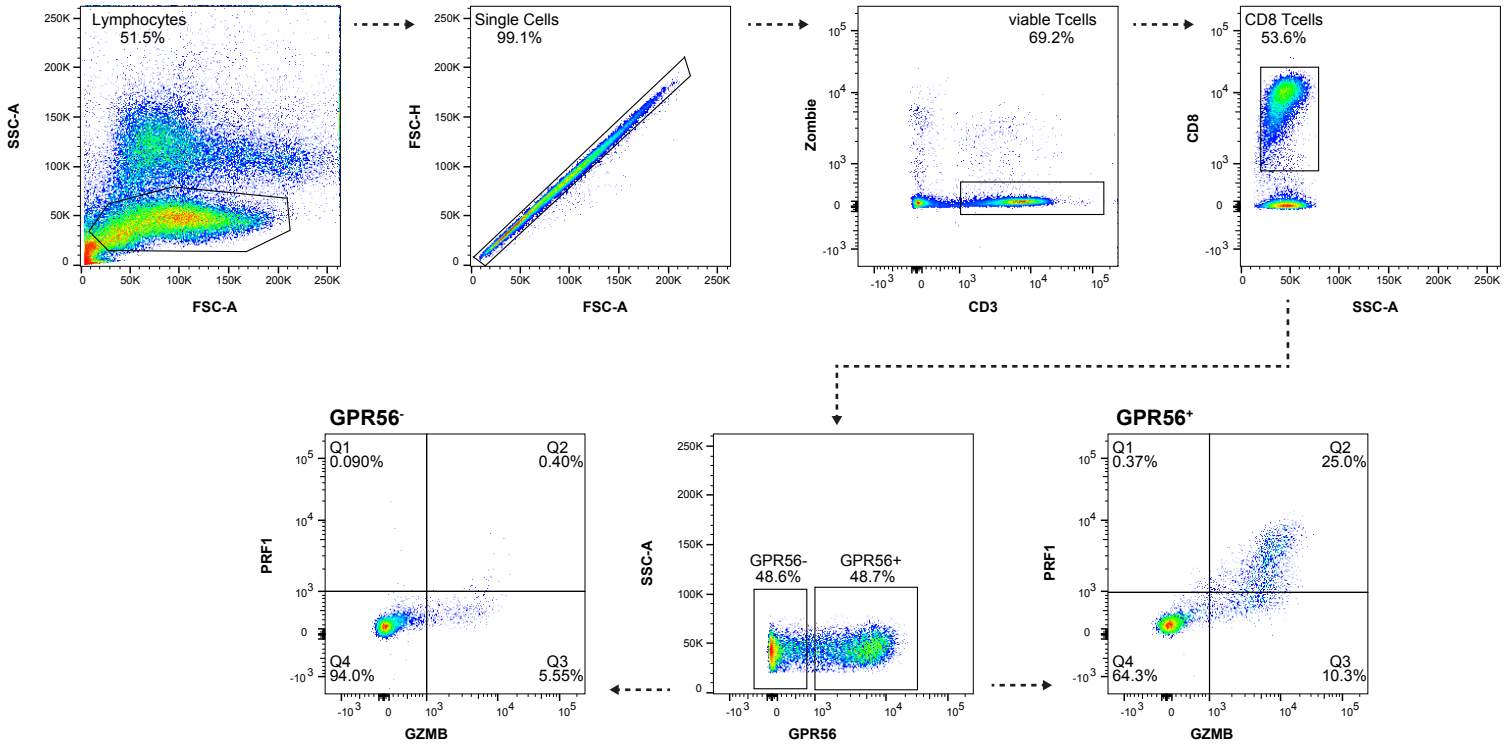

# Supplemental Figure 12

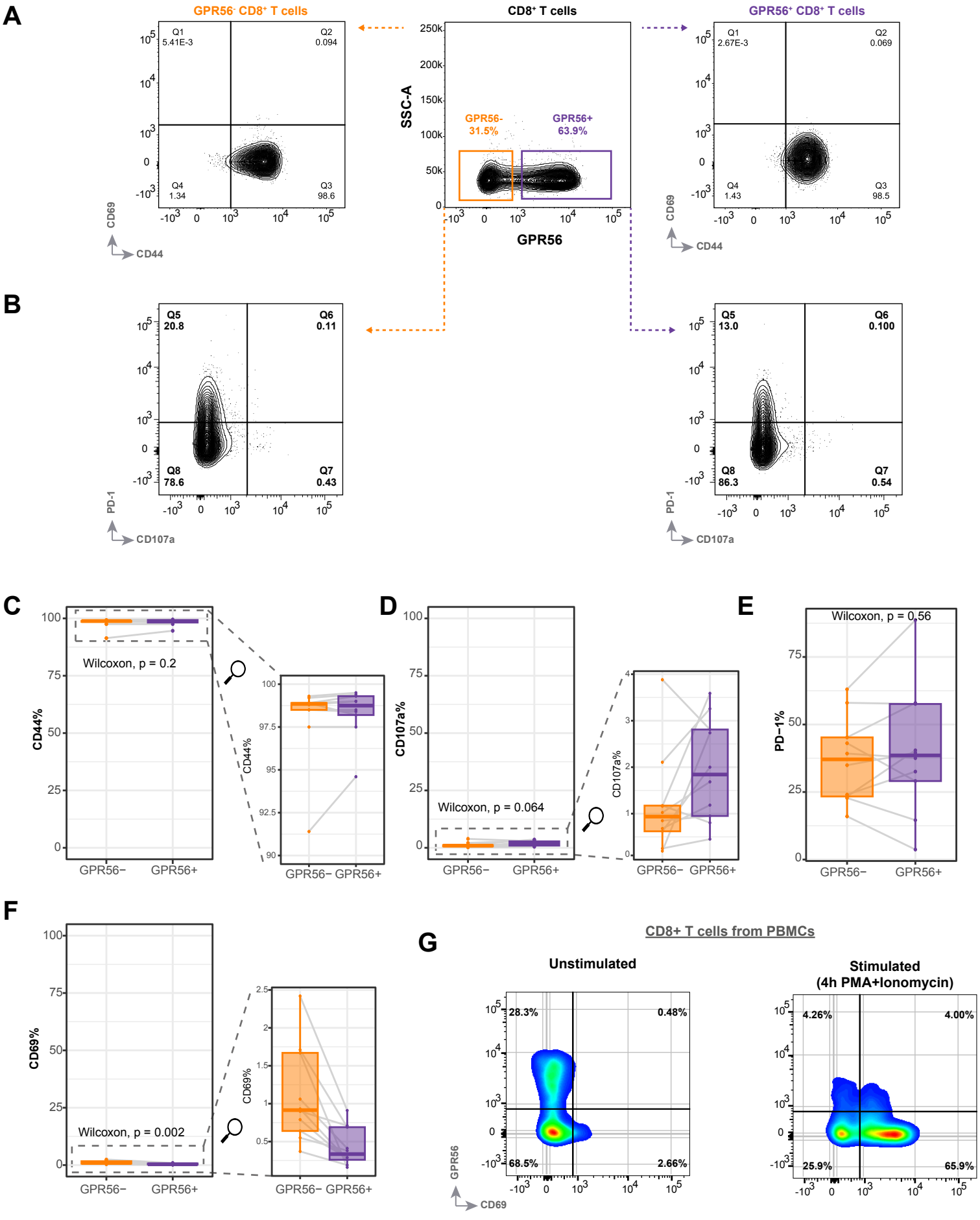

## Supplemental Figure 13

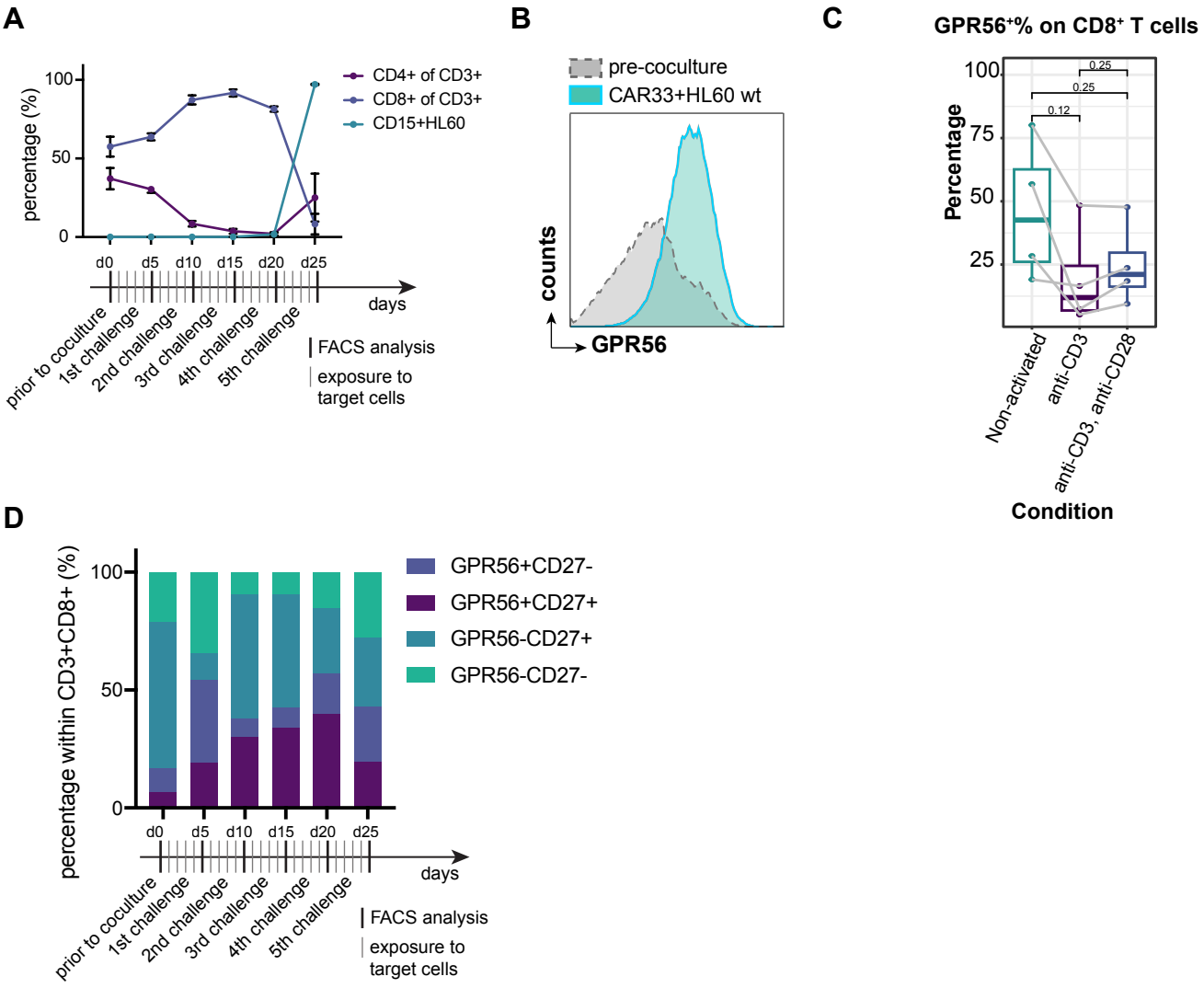

# Supplemental Figure 14

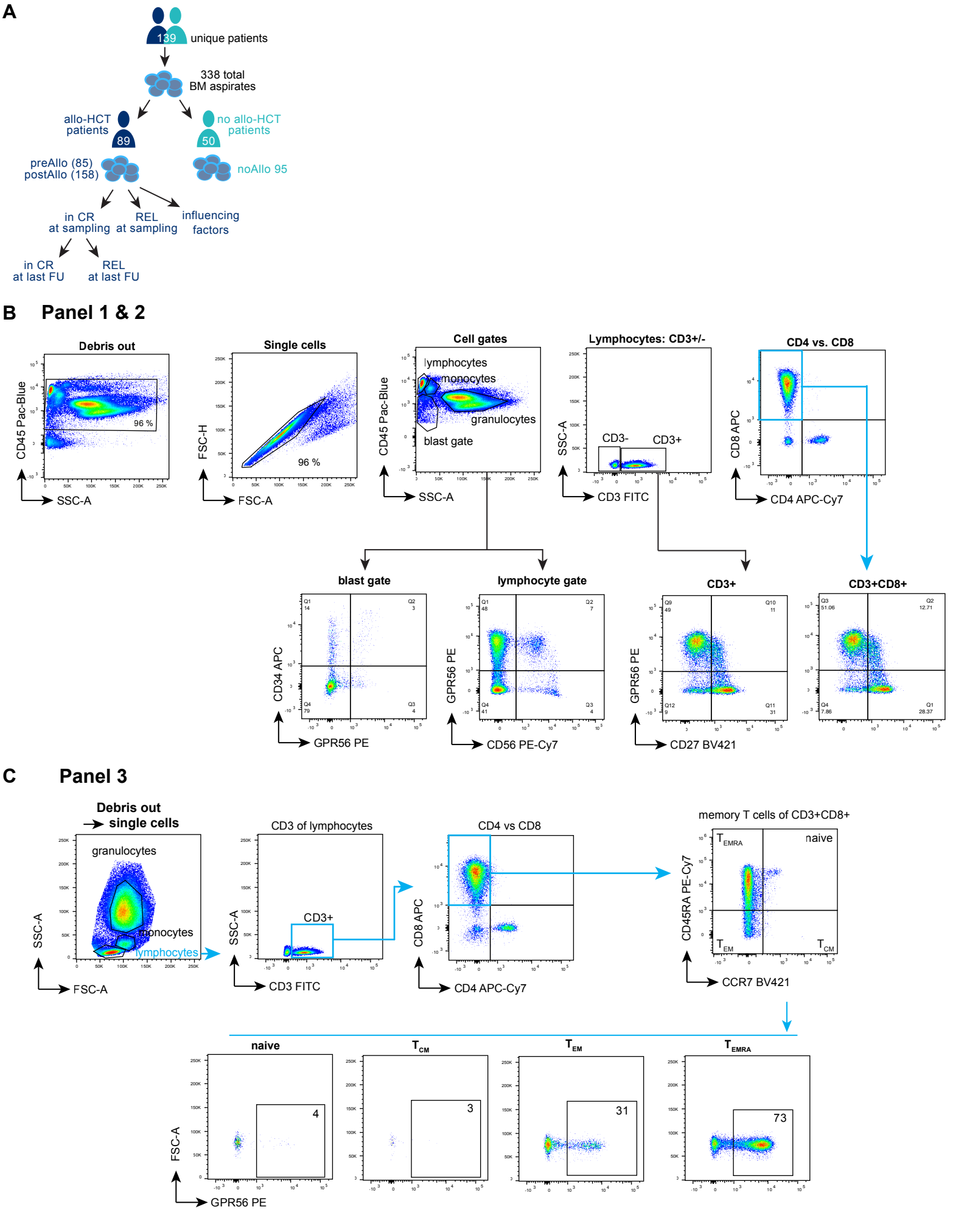

# Supplemental Figure 15

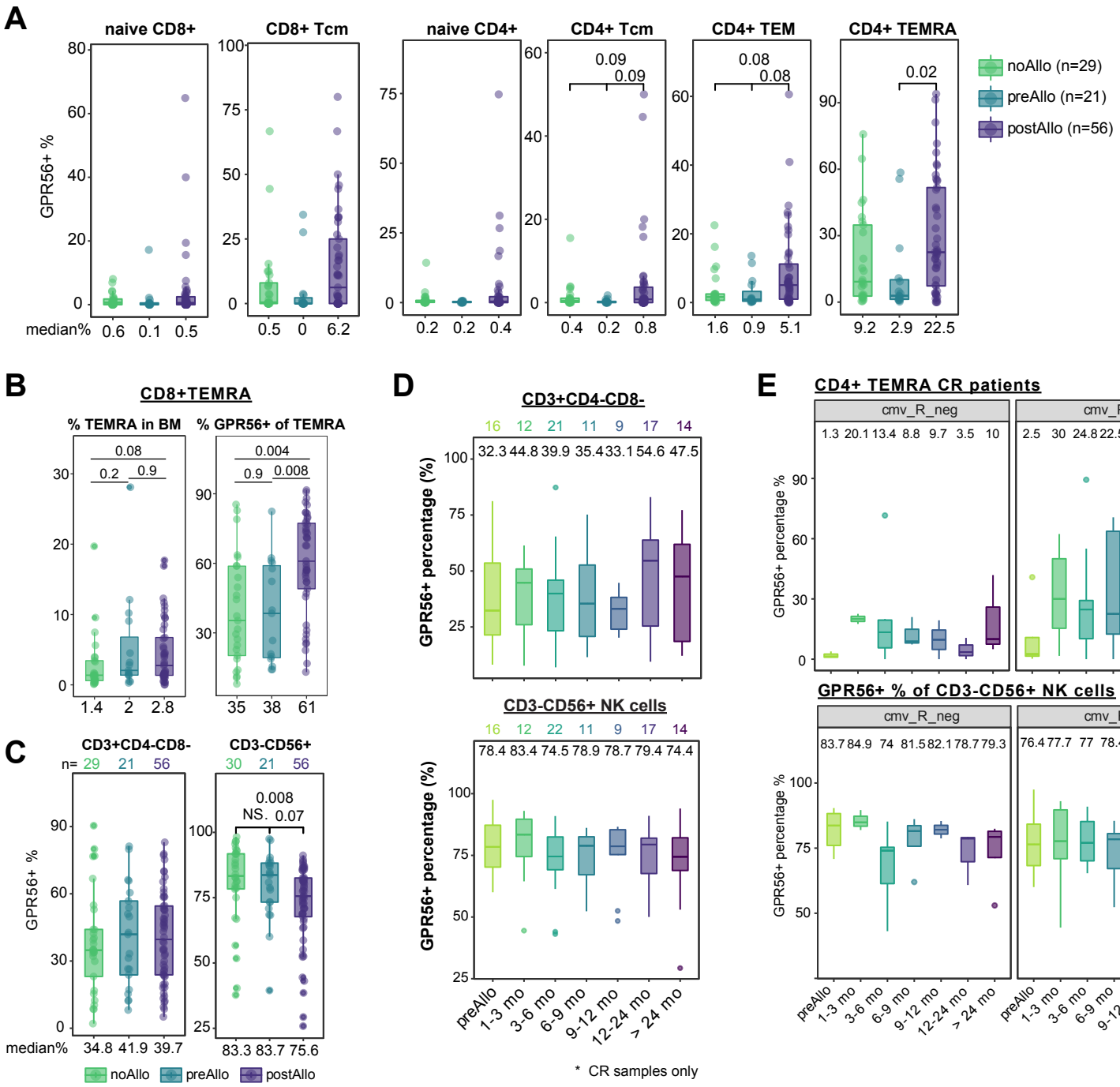

# Supplemental Figure 16

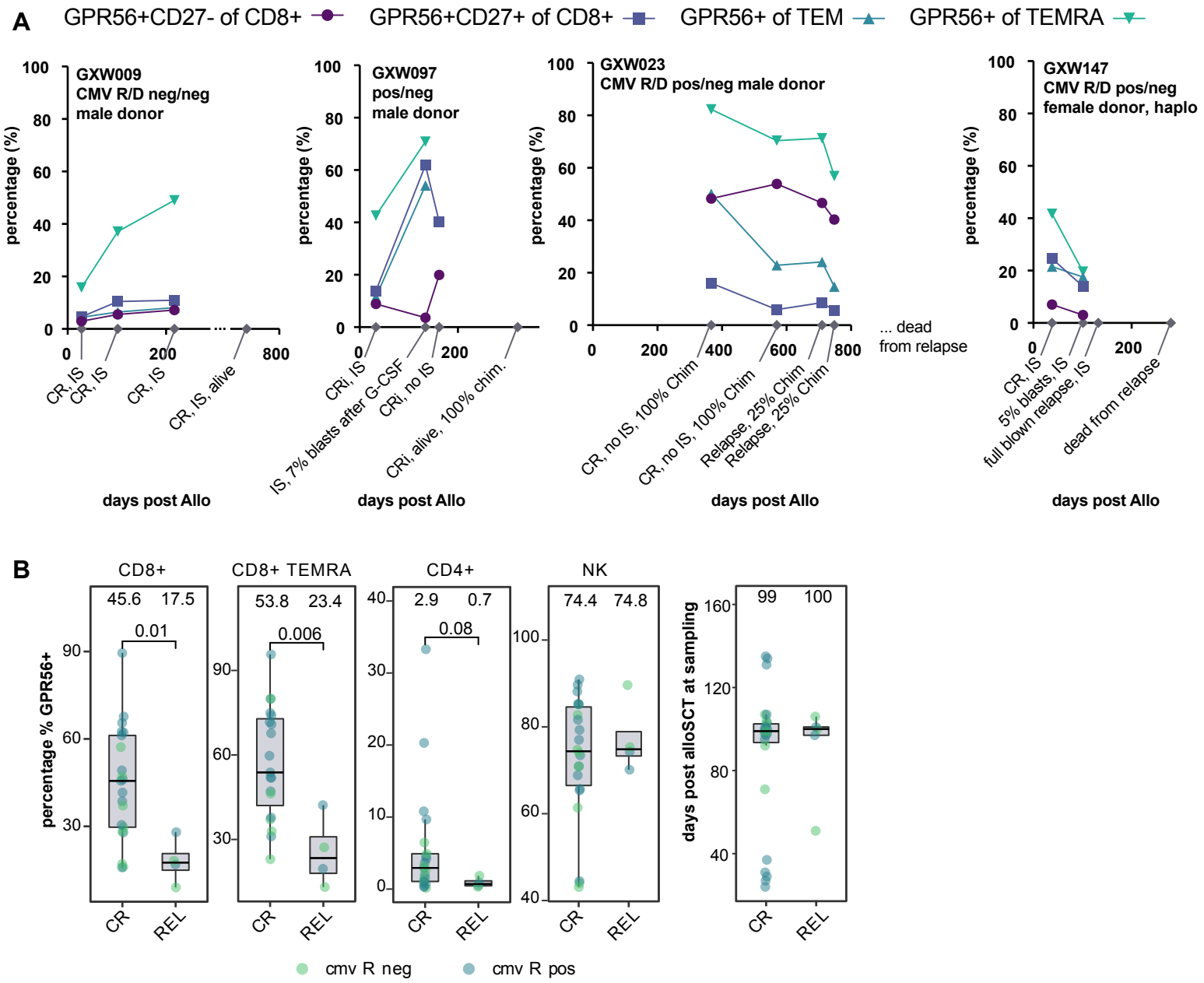


selection: only first 6 months post allo-HCT and in CR at sampling

# Supplemental Figure 17